Transcriptional Expression Changes During Compensatory Plasticity in the Central Nervous System of the Adult Cricket Gryllus Bimaculatus: I. Auditory System Plasticity in the Prothoracic Ganglia

Felicia Wang
Bowdoin College
Harrison Fisher
Bowdoin College
Maeve Morse
Bowdoin College
Lisa L. Ledwidge
Bowdoin College
Jack O'Brien
Bowdoin College
Sarah E . Kingston
University of Maine
Justin Beckman
Bowdoin College
Jasmine J. Johnson
Bowdoin College
Lyn S. Miranda Portillo
Bowdoin College
Tabarak N Al Musawi
Bowdoin College
Hadley Wilson Horch (hhorch@bowdoin.edu)
Bowdoin College

Research Article

Keywords: RNASeq, Transcriptome, Dendritic Plasticity, GO term analysis, Differential expression, Injury

Posted Date: February 19th, 2021

DOI: https://doi.org/10.21203/rs.3.rs-211260/v1

Transcriptional expression changes during compensatory plasticity in the central nervous system of the adult cricket *Gryllus bimaculatus*

I. Auditory system plasticity in the prothoracic ganglia

Felicia Wang, Harrison Fisher, Maeve Morse, Lisa L. Ledwidge, Jack O'Brien, Sarah E. Kingston^•, Justin Beckman, Jasmine J. Johnson, Lyn S. Miranda Portillo, Tabarak N. Al Musawi, Hadley Wilson Horch*,

Department of Biology, Bowdoin College, 6500 College Station, Brunswick, Maine 04672 USA.

^School of Marine Sciences and Darling Marine Center, University of Maine, 193 Clarks Cove Rd., Walpole, ME 04573 USA;
•University of California Santa Cruz, Ecology and Evolutionary Biology Department and UC Natural Reserves, 1156 High St, Santa Cruz, CA 95064 USA

*Correspondence to:
Dr. Hadley Wilson Horch, Department of Biology, Bowdoin College 6500 College Station, Brunswick ME 04011 USA. Phone: 207-798-4128; FAX: 207-725-3405; Email: hhorch@bowdoin.edu

Keywords:

RNASeq, Transcriptome, Dendritic Plasticity, GO term analysis, Differential expression, Injury

Abstract

Most adult organisms are limited in their capacity to recover from neurological damage. The auditory system of the Mediterranean field cricket, *Gryllus bimaculatus*, presents a compelling model for investigating neuroplasticity due to its unusual capabilities for structural reorganization into adulthood. Specifically, the dendrites of the central auditory neurons of the prothoracic ganglion sprout in response to the loss of auditory afferents. Deafferented auditory dendrites grow across the midline, a boundary they normally respect, and form functional synapses with the contralateral auditory afferents, restoring tuning-curve specificity. The molecular pathways underlying these changes are entirely unknown. Here, we used a multiple k-mer approach to re-assemble a previously reported prothoracic ganglion transcriptome that included ganglia collected one, three, and seven days after unilateral deafferentation in adult, male animals. We used EdgeR and DESeq2 to perform differential expression analysis and we examined Gene Ontologies to further understand the potential molecular basis of this compensatory anatomical plasticity. Enriched GO terms included those related to protein translation and degradation, enzymatic activity, and Toll signaling. Extracellular space GO terms were also enriched and included the upregulation of several protein yellow family members one day after deafferentation. Investigation of these regulated GO terms help to provide a broader understanding of the types of pathways that might be involved in this compensatory growth and can be used to design hypotheses around identified molecular mechanisms that may be involved in this unique example of adult structural plasticity.

Background

Most adult organisms, especially mammals, are limited in their capacity to adapt and recover from neurological damage (1,2). The Mediterranean field cricket, *Gryllus bimaculatus*, provides a model of neuroplasticity due to its demonstrated ability to compensate for neuronal damage with novel dendritic growth and synapse formation, even into adulthood. Specifically, the central auditory system, much of which resides in the prothoracic ganglion, reorganizes in response to deafferentation caused by unilateral transection of auditory afferents in the adult (3–5).

In *G. bimaculatus*, auditory information is transduced by the auditory organs, located on the prothoracic limbs. Auditory afferents receive the sensory stimuli and convey this information into the prothoracic ganglion where they form synapses with several different auditory neurons (6,7). These neurons exist as mirror image pairs and their dendritic arbors remain localized ipsilateral to the auditory input, typically not projecting contralaterally across the midline (8). However, previous research has shown that after amputation of the prothoracic leg in the adult, which removes the auditory organ and severs the afferents, the deafferented dendrites of the ipsilateral auditory neurons sprout across the midline and form functional synapses with the intact auditory afferents on the contralateral side. This reorganization is evident whether deafferentation occurs in larvae (9,10) or adults (3–5). Various aspects of the physiological consequences of this compensatory behavior have been studied (3,9,10), however little is known about the molecular pathways and mechanisms underlying this growth.

Although the genome has only just become publicly available (11), various *de novo* transcriptomes have been created for use in this species (12–14). Recently, a *de novo* transcriptome of the prothoracic ganglion was assembled in an attempt to understand the

molecular basis of the compensatory response (15). This transcriptome was built with RNA from individual prothoracic ganglia of both control and deafferented adult male crickets. Initially, this transcriptome was assembled and mined for the presence of developmental guidance molecules. These guidance molecules are known to play a well-conserved role in regulating the specific growth of axonal and dendritic projections during the development of many species (16,17). While these molecules have mainly been studied for their role in development, it has also been suggested that alterations in their expression may influence the ability of axons and dendrites to recover from injury in adulthood (15,18–20). Mining this cricket transcriptome revealed that many well-conserved developmental guidance molecules, including slit, ephrins, netrins, and semaphorins, were present within the adult prothoracic transcriptome (15). However, it is still unknown whether the expression of these transcripts, or any other transcripts, are significantly altered during this compensatory growth process.

The goal of this study was to better understand the underlying molecular control of the compensatory growth behavior observed in the cricket. We assembled a new, more representative and less redundant transcriptome of the cricket prothoracic ganglion using multiple k-mer values during the assembly process. We also utilized the Evidential Gene *tr2aacdsmRNA* classifier to reduce redundancies (21). This new transcriptome was used to analyze changes in expression levels one, three, and seven days post-deafferentation. The identified genes were then analyzed using GO annotation analysis to determine the classes of genes that are differentially regulated over the course of the injury response. By performing this analysis, it was possible to discover changes in gene expression that occur during the compensatory growth response, allowing for insights into possible pathways or key molecules critical to this process.

Results and Discussion

Transcriptome Assembly and Analysis

This transcriptomic study focused on the cricket, *Gryllus bimaculatus*, whose nervous system has been shown to have an unusual level of adult structural plasticity (3–5). We deafferented sensory neurons, including the auditory neurons, in the prothoracic ganglion of the adult cricket, by unilateral amputation of the prothoracic leg at the femur. Control amputations consisted of removal of the distal tip of the tarsus. We harvested prothoracic ganglia one, three, and seven days post-amputation. These time points were designed to capture transcriptional changes in response to the injury (one day), during initial sprouting (one and three days), growth across the midline (three and seven days), and *de novo* synapse formation (3,22).

Although a *G. bimaculatus* prothoracic ganglion transcriptome from this tissue was previously assembled, analyzed, and mined (15), the present study re-assembled a new transcriptome based on those original cleaned and trimmed RNA-Seq reads. Five individual *de novo* transcriptomes were built in Trinity using five different k-mer lengths (21, 25, 27, 30, and 32). Transcriptome construction with longer k-mer lengths produces more reliable contigs, though biased toward highly expressed transcripts. In a complementary fashion, using a shorter k-mer length produces a more exhaustive set of contigs though also one more prone to noise (23,24). This trade-off between bias and noise induced by the choice of k-mer length suggests how a higher quality *de novo* assembly can be derived by integrating multiple k-mer lengths into an analysis (23). By combining results across k-mer lengths, we ensured that a complementary selection of contigs was included in the analysis (23,25,26). Correspondingly, we combined the five assemblies into a single reference transcriptome and subsequently filtered redundancies and fragments.

The individual assemblies had an N50 ranging from 1,219 - 2,341, with the longer k-mer assemblies yielding a longer N50 (Table 1). The median, average, and maximum contig length also increased as the k-mer length was increased. The total number of Trinity "genes" ranged from 283,278 to 351,829, with higher k-mer assemblies yielding fewer predicted genes. The GC content for each assembly remained roughly constant, between 40-41%. The overall alignment was greater than 98%, with multimapping percentages between 90.04-93.33% (Table 1). This high multimapping percentage can likely be attributed to the Trinity assembly process, which is conservative in its separation and identification of unique transcripts, producing high intra-assembly redundancy (27).

Table 1: Individual k-mer assembly details.

	k-mer = 21	k-mer = 25	k-mer = 27	k-mer = 30	k-mer = 32
Total # bases assembled	293,992,611	404,116,670	408,831,054	406,965,539	403,174,726
Total # assembled contigs	405,638	438,593	431,712	415,901	407,158
Total # Trinity "genes"	351,829	302,633	297,584	288,135	283,278
Average contig length (bp)	724.77	921.39	946	978.52	990.22
Median contig length (bp)	376	397	397	399	400
Maximum contig length (bp)	37,575	44,287	44,328	44,352	44,331
N50 (bp)	1219	2000	2141	2272	2341
GC count for assembly (%)	40.94	40.39	40.32	40.19	40.14
Overall alignment	98.61	98.58	98.66	98.71	98.74
Reads mapped 1 time (%)	4.4	3.69	2.71	2.08	2.55
Reads mapped >1 time (%)	90.04	90.95	92.21	93.33	92.9

Table 1. Summary metrics for five different de novo transcriptomes built with five different k-mer lengths.

The five transcriptomes were combined to generate a transcriptome with a total of 2,099,002 contigs (Figure 1), presumably many of which were redundant. We used the EvidentialGene *tr2aacdsmRNA* classifier to filter the redundancies within our transcriptome, which were present due to both intra- and inter-assembly redundancies (21). The EvidentialGene program employs an algorithm that operates on the open reading frames of the contigs to generate a non-redundant transcriptome containing the optimal set of transcripts based on biological relevance and coding potential (21,28). This program is often used in 'over-assembly' procedures where multiple assemblies are combined (29–31). With our multi-k-mer assembly, EvidentialGene produced a

main ‘okay’ set, containing 55,895 contigs, and an alternative ‘okalt’ set, containing 143,364 contigs, which were combined to produce a final transcriptome with a total of 199,357 contigs, reducing the overall number of contigs by 90.5%. BLAST searches across all the contigs yielded matches for 127,324 transcripts, a 63.87% BLAST hit rate for the entire transcriptome. The number of Trinity predicted genes after running EvidentialGene dropped slightly to 132,972. The multimapping percentage was reduced from approximately 90% to around 21%.

To check the accuracy of the sequences predicted in the transcriptome, we used Sanger sequencing to independently confirm the sequences of six randomly selected transcriptome transcripts. Of these six, four of them were predicted to contain complete open reading frames (ORFs), and two were missing the 3’ end. We analyzed 14,299 nucleotides of 15,478 predicted base pairs (92%). The number of substitutions (16), insertions (84), and deletions (0) were noted; overall, these differences accounted for approximately ~0.1% of the sequenced nucleotides (data not shown). A few additional randomly selected sequences were highly repetitive and were not amenable to Sanger sequencing; we did not proceed with an analysis of any of these candidates.

Differential expression during compensatory plasticity

To determine genes that were differentially regulated during compensatory plasticity, the reads for each of the 16 Illumina libraries, which excluded the two outliers and three backfill libraries (see Methods), were mapped back to our multiple k-mer transcriptome creating a counts matrix. Pairwise comparisons of normalized counts data from deafferented *vs*. control crickets were performed at each time point using both algorithms, EdgeR and DESeq2 (See Supplemental Materials). The distribution of differentially expressed genes was initially visualized using volcano plots (Figure 2). These plots revealed slightly different distributions of upregulated versus downregulated genes between the two programs. Overall, however, we saw strong

correlations between these two programs for all time points (Figure 3), with the exception of a few of the high fold-change candidates. Within this range, EdgeR was consistently more conservative than DESeq2, which was especially true for a small number of upregulated candidates (Figure 3a-c).

The majority of the transcripts were upregulated in the 2 to 4-fold range at one day (59% of the transcripts), three days (55% of the transcripts), and seven days (45% of the transcripts). The next largest group of transcripts was upregulated at 0 to 2-fold at one day (33% of transcripts), three days (41% of transcripts), and seven days (39% of transcripts). For those candidates that were downregulated, a majority of them at one day (63%) and three days (86%) were downregulated less than 2-fold. At seven days, the bulk of candidates (70%) were downregulated 2 to 4-fold. Analysis of 10 of the transcripts at each time point with the largest fold changes revealed that most were unidentified and did not match anything in the NCBI database when BLASTed. A few of these transcripts did have BLAST hits, such as a mucin-5AC-like (down at one day), larval cuticle protein-3-like (down at seven days), and hypothetical accessory gland protein (up at three and seven days).

Using EdgeR, 261 genes were found to be downregulated at one day post-deafferentation, 1,675 genes were downregulated at three days post-deafferentation, and 580 genes were downregulated at seven days post-deafferentation (Figure 4a). Additionally, 2,234 genes were determined to be upregulated at one day post-deafferentation, 1,860 genes upregulated at three days post-deafferentation, and 290 genes upregulated at seven days post-deafferentation (Figure 4b).

A similar pairwise comparison of deafferented versus control crickets was performed using the DESeq2 software and revealed that 985 genes were downregulated at one day post-

deafferentation, 3,049 genes were downregulated at three days, and 448 genes were downregulated at seven days (Figure 4c). Additionally, 3,589 genes were upregulated at one day post-deafferentation, 1,424 genes were upregulated at three days, and 535 genes were upregulated at seven days (Figure 4d).

From these sets, simple comparisons were created to determine the number of genes upregulated and downregulated across multiple timepoints. In EdgeR, there were four genes downregulated at one and three days, two genes at one and seven days, two genes at three and seven days, and 0 genes differentially downregulated across all three time points (Figure 4a). For the upregulated genes, there were 174 genes differentially regulated at one and three days, 18 genes at one and seven days, 18 genes at three and seven days, and 32 genes at all three time points (Figure 4b). Comparing the DESeq2 sets of genes across multiple timepoints showed that there were nine genes downregulated at one and three days, one gene downregulated at one and seven days, four genes downregulated at three and seven days, and 0 genes downregulated at all three timepoints (Figure 4c). Additionally, 168 genes were found to be upregulated at one and three days, 73 genes at one and seven days, 23 genes at three and seven days, and 40 genes at all three time points (Figure 4d).

Finally, simple comparisons were performed between EdgeR and DESeq2 with genes determined to be differentially expressed at each of the three times points. For downregulated genes, 180 were identified at one-day post deafferentation, 1,604 at three days, and 367 at seven days. For upregulated genes, 2,099 were identified at one-day post deafferentation, 1,043 at three days, and 272 at seven days (Figure 5). The genes found to be differentially regulated by both programs were used for further analysis.

DESeq2 and EdgeR are the leading programs used for the analysis of RNA-Seq data, with thousands of reports both using these methods for analyzing differential expression and comparing their computational methods (32,33). While both operate under the hypothesis that the majority of genes are not differentially expressed, they employ different computational methods, especially with respect to the normalization process, to determine differentially expressed genes (33). EdgeR and DESeq2 both use a normalization by distribution method, but EdgeR relies on the Trimmed Mean of the M-values method, whereas DESeq2 uses a Relative Log Expression method (34–37). Since different methods rely on differing assumptions in order to identify differentially expressed genes, the results will vary slightly. One experiment comparing EdgeR and DESeq2 found relatively similar lists of differentially expressed genes produced by the two programs, with EdgeR producing more conservative, smaller gene lists (32). In this study we decided to use two different programs to conduct the differential expression analysis in order to create a smaller, more conservative set of genes for future functional analyses. Out of the six comparisons between EdgeR and DESeq2 (upregulated and downregulated at one, three, and seven days post injury), four out of the six resulted in EdgeR producing a smaller set of genes than DESeq2 (Figure 5), in line with the study by Raplee and colleagues (32). Although the two programs generated varying numbers of differentially regulated genes, similar patterns in relative numbers were observed. Both programs showed a decrease in the number of genes upregulated across time. For the downregulated genes, a peak in the number of differentially regulated genes was found at three days post injury. This similarity was expected given the relative similarity and previous studies of both analysis programs.

BLAST and Gene Ontology Annotations

Once we had identified a conservative set of transcripts predicted to be differentially regulated, we used BLAST2GO (38) to try to identify them. Not all the transcripts inputted into the BLAST2GO program resulted in BLAST hits and/or GO annotations. At one day downregulated, 71% of genes had both BLAST and GO results and an additional 10% had only BLAST hits. At three days downregulated, 36% of genes had both BLAST and GO results and an additional 6% had only BLAST hits. At seven days downregulated, 31% of genes had both BLAST and GO results and an additional 6% had only BLAST hits. For the one day upregulated, 53% of genes had both BLAST and GO results and an additional 10% had only BLAST hits. At three days upregulated, 59% of genes had both BLAST and GO results and an additional 15% had only BLAST hits. At seven days upregulated, 50% of genes had both BLAST and GO results and an additional 15% had only BLAST hits (Figure 6).

For the six lists of differentially expressed transcripts, there was a range between 37-81% of transcripts having BLAST hits against the nr database and 23-62% against the manually curated and annotated Swiss-Prot database. After mapping with GO terms, this was reduced to about 31-59%. This left close to half of the differentially regulated transcripts with no functional information. These transcripts could represent uncharacterized proteins, which may or may not be playing an important role in the compensatory growth response. Since we performed a BLASTx looking at proteins, it is also possible that these transcripts are non-coding RNAs. Although polyA selection was used as part of the RNA-Seq process, this may not be completely efficient in removing all non-coding RNAs, specifically long non-coding RNAs (39,40). Finally, it is also possible that there were issues within these transcripts themselves, either due to an error

during the assembly process or the sequences being too short to be matched with confidence. Regardless, we completed no further analysis of these transcripts.

One interesting group of proteins that was found to be upregulated at one day was the protein yellow family. Protein yellow belongs to the major royal jelly protein family and are secreted proteins found in the extracellular region (41). Protein yellow was first characterized in *Drosophila melanogaster* for its role in pigmentation (42). Other research in honeybees revealed the importance of royal jelly proteins in development and social behavior in addition to a possible role in the CNS (41,43). However, the function of these yellow/royal jelly proteins is not completely understood (42). While the role of these proteins in crickets is unclear, they were statistically differentially regulated and would be an interesting molecular family to investigate for their role in deafferentation-induced plasticity.

GO Term Distributions

Based on a preliminary grouping of GO terms by the three root classes, it appeared that several classes of GO terms were found to be associated with our differentially expressed genes (Figure 7). While the top five represented GO terms encompassed most of the GO terms in the cellular component category, there was a much broader range of GO terms represented in the molecular function and biological process categories

Web Gene Ontology Annotation Plot (44,45) was used to plot a broader distribution of GO terms and visually compare annotations among timepoints (Figure 8). Cellular component, molecular function, and biological process were displayed on traditional WEGO histograms (Figure 8a, b). The percentage of genes indicates the percentage of the genes within a given list that were annotated with the given GO term or one of the child nodes of the term. GO terms with

higher percentage representation included terms describing membrane-related components as well as terms related to catalytic activity, binding, and metabolic and cellular processes.

Gene Ontology Categories

We examined whether any of the candidate GO terms we identified here were associated with injury-related plasticity paradigms identified in other species. For example, perhaps successful regeneration after injury depends on the recapitulation of developmental proteins that promote neurogenesis (46) or guide axons and dendrites (18). If these molecular strategies were important for the plasticity observed in the cricket, we would predict that we might see changes in the expression of transcription factors involved in neurogenesis and/or the regulation of several classes of guidance cues normally involved in midline control in insect embryos. When searching our differentially regulated candidates, a few genes downregulated at three days were associated with GO terms that were related to neurogenesis (**GO:0007465**: R7 cell fate commitment and **GO:0045466**: R7 cell differentiation). We found only one transcript that was annotated with an axon guidance-related GO term, which was identified as a "twitchin-like protein," (Table 2). Twitchin/Unc-22 is a large protein kinase thought to be important in muscle development and function (47).

An initial study of our original single k-mer transcriptome explored this developmental recapitulation hypothesis by mining the transcriptome for the presence of various guidance molecules (15). Though transcripts corresponding to the signaling families, slit, netrin, ephrin, and semaphorin were identified within this adult transcriptome, the BLAST and Gene Ontology analyses performed here did not identify an abundant number of guidance molecules as differentially regulated. Despite this result, however, it is important to note that the transcriptome and differential expression analysis were performed on the whole prothoracic ganglion, which

295 could mask important changes that occur in single cells after deafferentation, such as in
296 ascending neuron 1 and 2 (AN-1 and AN-2). Single cell RNA-Seq analysis of the ANs could
297 help to determine whether there are changes in expression occurring on a smaller anatomical
298 level.

299 Based on results from different types of injury model systems in other organisms,
300 additional functional categories that we hypothesized could change during the compensatory
301 growth response were those related to apoptosis (48,49) and Wnt signaling (50). In our
302 differentially expressed gene sets we did not find enrichment in terms related to apoptosis.
303 Searching our results for Wnt-related GO terms, revealed a few genes annotated with Wnt
304 pathway members at 3 days post deafferentation (Table 2). These genes had a top BLAST hit of
305 atrial natriuretic peptide-converting enzyme isoform X1, Frizzled-4, and secreted frizzled-related
306 protein 5-like.

307 We looked for the presence of a number of additional groups of proteins that influence
308 neuronal morphogenesis, plasticity, or remodeling (Table 2). For example, the matrix
309 metalloproteases (MMPs) are required for axonal guidance (51) as well as dendritic remodeling
310 during metamorphosis in *Drosophila melanogaster* (52). Importantly, the expression of some
311 MMPs appear to contribute to poor recovery after spinal cord injury in mammals (53). We did
312 not find enrichment in any of these terms at any time point (Table 2), indicating that the injury-
313 induced anatomical plasticity in the cricket may rely on different pathways than have been
314 identified in other species. Furthermore, it is notable that factors, such as MMPs, that can restrict
315 growth or contribute to pruning in other organisms are not upregulated upon injury in the cricket.

316 Several GO terms associated with the candidates found in a previous subtraction
317 hybridization study (54) were also found to be differentially expressed in the present experiment,

often showing significant changes in expression at the three- and seven-day post-deafferentation time point (Table 2, bold). These include oxidoreductase, alpha-amylase, endoglucanase, and alcohol dehydrogenase. As noted by Horch and colleagues (54), many of these enzymes have been observed in the hemolymph of insects and play a role in metabolism and immune response. Although it is possible that these findings are due to contaminants during the extraction of the prothoracic ganglion, the results would imply that the extractions differed between control and experimental animals in multiple experiments. Given that the differential expression of several enzyme transcripts was found both in this study and in the SSH study, it is less likely that these enzymes are artifact or contamination effects. Particularly, several differentially regulated transcripts were associated with oxidoreductase activity across all time points. The BLAST hits of these transcripts showed some of the enzymes to be retinal dehydrogenases. Retinal dehydrogenase along with alcohol dehydrogenase, another regulated GO term, are involved with the production of retinoic acid. Retinoic acid has been shown to be involved with development, regeneration, synaptic plasticity, and neurite outgrowth (55–57) implying that regulation of retinoic acid production may influence these processes. Another class of oxidoreductases that appeared abundant within the BLAST hits was the cytochrome P450 family. Cytochrome P450 is a superfamily of monooxygenase enzymes and several families of cytochrome P450 exist in insects. These enzymes are known to have a variety of functional roles in insects including growth and development (58). Cytochrome P450 has also been shown to regulate ecdysone signaling in insects, including crickets (59,60). Ecdysone signaling is crucial for developmental processes and morphogenesis, but has also been shown to be important in the dendritic remodeling of *Drosophila melanogaster* sensory neurons (52,59). While these protein families

represent some of the transcripts annotated with “oxidoreductase activity”, given the wide range of such transcripts, it is difficult to discern the role of all of the regulated proteins.

Table 2: Evaluation of the number and fold-change of GO terms of interest.

GO ID	GO Term	Down 1	Down 3	Down 7	Up 1	Up 3	Up 7
GO:0007411	**axon guidance**	N/A	N/A	N/A	N/A	**1 (3.10)**	N/A
GO:0048813	dendrite morphogenesis	N/A	N/A	N/A	N/A	N/A	N/A
GO:0022008	**neurogenesis**	N/A	**6 (1.00 ± 0.01)**	N/A	N/A	**1 (3.10)**	N/A
GO:0008219	cell death	N/A	N/A	N/A	N/A	N/A	N/A
GO:0099544	perisynaptic space	N/A	N/A	N/A	N/A	N/A	N/A
GO:1990773	MMP secretion	N/A	N/A	N/A	N/A	N/A	N/A
GO:0198738	**cell-cell signaling by wnt**	N/A	**4 (-1.99 ± 0.34)**	N/A	N/A	**1 (1.28)**	**1 (1.20)**
GO:0004185	serine-type carboxypeptidase activity	N/A	N/A	N/A	N/A	N/A	N/A
GO:0003735	ribosomal constituent	N/A	N/A	N/A	N/A	N/A	N/A
GO:0003743	translation initiation factor activity	N/A	N/A	N/A	N/A	N/A	N/A
GO:0008135	**translation factor activity, RNA binding**	N/A	N/A	N/A	N/A	N/A	**12 (2.85 ± 0.24)**
GO:0008106	**alcohol dehydrogenase (NADP+) activity**	N/A	N/A	N/A	**3 (1.26 +/- 0.01)**	N/A	N/A
GO:0004556	**alpha-amylase activity**	N/A	N/A	**8 (-2.77 ± 0.27)**	N/A	**13 (2.65 ± 0.61)**	N/A
GO:0015927	trehalase activity	N/A	N/A	N/A	N/A	N/A	N/A
GO:0016491	**oxidoreductase activity**	**4 (-2.38 ± 2.24)**	**112 (-1.40 ± 0.43)**	**14 (-2.82 ± 0.45)**	**175 (2.45 ± 0.92)**	**124 (2.38 ± 0.90)**	**7 (3.48 ± 1.69)**
GO:0008810	**cellulase activity (endoglucanase)**	N/A	N/A	**3 (-2.43 +/- 0.30)**	N/A	**1 (1.97)**	N/A
GO:0003796	lysozyme activity	N/A	N/A	N/A	N/A	N/A	N/A
GO:0004129	cytochrome-c oxidase activity	N/A	N/A	N/A	N/A	N/A	N/A
GO:0016567	**protein ubiquitination**	**1 (-1.60)**	**1 (-1.24)**	N/A	**3 (2.53 ± 0.29)**	**11 (2.15 ± 0.76)**	**22 (1.91 ± 0.10)**
GO:0019783	ubiquitin-like protein specific protease activity	N/A	N/A	N/A	N/A	N/A	N/A

Table 2: Number of transcripts associated with the selected GO terms, including any child term of the GO term, at each time point. For each represented GO term, the average +/- standard deviation of the log2foldchange across the transcripts is given in parentheses. GO Terms in bold indicate significant changes in expression. GO IDs in italics were selected because similar transcripts were present in a prior SSH study (54).

Gene Ontology Enrichment Analysis

Metascape (61) was used to determine enriched GO terms across the differentially expressed gene lists. Differentially expressed genes were first reBLASTed against the curated Swiss-Prot database to retrieve appropriate gene identifiers. Similar ratios of BLAST hit percentages across timepoints were observed against Swiss-Prot as with the nr database, however, the percentage of genes with BLAST hits was lower when BLASTed against Swiss-Prot versus the nr database (Table 3).

Table 3: Comparison of the percentage of genes with BLAST hits in the nr database vs. Swiss-Prot.

	nr	Swiss-Prot
Down 1	81%	59%
Down 3	42%	36%
Down 7	37%	23%
Up 1	62%	59%
Up 3	73%	62%
Up 7	65%	57%

Enrichment analysis by Metascape showed the most enriched terms at three days post-deafferentation across both upregulated and downregulated genes. Examining the multi-list analysis, there were 22 enriched GO terms found including those related to morphogenesis, extracellular space, and neuron fate commitment (Figure 9). No enriched GO terms were found in the upregulated gene set at seven days post-deafferentation.

One category of interest that was revealed in this enrichment analysis was the GO Term "Regulation of Toll-signaling pathway." Toll receptors are most commonly associated with their function in immunity and development, however, research in *Drosophila melanogaster* suggests that they may also play a role in regulating cell number, connectivity, and synaptogenesis (62). Activation of Toll receptors can regulate cell number through either neuroprotective and cell survival or pro-apoptotic functions, depending on the receptor type. These functions of Toll receptors were shown to exist in both development and adulthood (63). Toll receptors, specifically Toll-6 and Toll-7, have also been shown to have neurotrophic receptor-like functions through their ability to bind multiple ligands, including neurotrophin-like proteins in invertebrates (64). Neurotrophins are known to regulate cell proliferation and neuronal survival and development, thereby suggesting an important role for Toll receptors in neuronal systems (63,64). Furthermore, in *Drosophila melanogaster* the receptor Toll-8 was shown to positively regulate synaptic growth through a retrograde neurotrophin-like signaling mechanism (65). These studies show that Toll signaling may play an important role in regulating structural plasticity in invertebrates and, given their enrichment in our differentially regulated gene set, may be crucial to the dendritic reorganization observed in the cricket.

Conclusions

Unilateral tympanal organ removal in the cricket, *Gryllus bimaculatus*, leads to a robust reorganization of dendrites in the auditory system of the prothoracic ganglion. This novel growth and *de novo* synapse formation restores the ability of the deafferented neurons to respond to sound. Our transcriptomic analyses identified thousands of transcripts up- and down-regulated after deafferentation. We highlight transcriptional changes related to protein translation and

degradation, enzymatic activity, and Toll signaling that appear to be enriched after deafferentation. The data presented here allows the development of targeted hypotheses that could elucidate the mechanisms responsible for the deafferentation-induced synaptic plasticity in the auditory system of crickets. The mechanisms at play here can be compared and contrasted with those identified in the terminal ganglion of the cricket after unilateral loss of a cercus.

Methods

Animals, injury, and library preparation

Prothoracic ganglia from approximately 60 adult, male Mediterranean field crickets, *Gryllus bimaculatus* were harvested and 21 individual ganglia were ultimately used as the sources of RNA for this transcriptome (15). Male crickets that were adults for 3-5 days received either a control amputation of the distal segment of the left tarsus ("foot chop" control crickets), or the left prothoracic leg was severed mid-femur removing the auditory organ and deafferenting the ipsilateral central auditory neurons ("deafferented" experimental crickets). Males were chosen due to the potential sexual dimorphism in rates of dendritic growth after deafferentation (22). (15). Several crickets were prepared for backfill as previously described (15). Prothoracic ganglia were removed from these crickets 1, 3, or 7 days after amputation at the femur or tarsus and total RNA was purified as previously described.

The QIAGEN RNeasy Lipid Tissue Minikit was used to purify total RNA from each sample individually. RNA concentrations were assessed after TURBO DNA-free treatment (Ambion by Life Technologies) with a nanospectrophotometer (Nanodrop, Thermo Fisher Scientific) or a fluorometer (Qubit, Thermo Fisher Scientific). An Agilent 2100 Bioanalyzer (Applied Biosystems, Carlsbad, CA) was used to further assess sample quality. Based on

412 evaluation of RNA quality and concentration of individual ganglion samples, the best 3 samples
413 for each condition were selected for sequencing. Standard Illumina paired-end library protocols
414 were used to prepare samples. The Illumina Hiseq 2500 platform, running v4 chemistry to
415 generate ~25M paired end reads of 100bp in length for each sample, was used to sequence the
416 RNA (15).

417 ***Transcriptome assembly***

418 Trinity software (Trinity-v2.6.5) was run using previously processed and filtered reads of
419 prothoracic ganglion libraries (15). A multi-k-mer assembly was created by building five *de novo*
420 transcriptomes using a single k-mer length (21, 25, 27, 30, 32) and subsequently combining
421 them. The following parameters were used: minimum contig length of 200, library normalization
422 with maximum read coverage 50, RF strand specific read orientation, maximum memory,
423 250GB, and 32 CPUs. Individual assemblies were analyzed using the *TrinityStats.pl* script and
424 alignment statistics were obtained using Bowtie2 (v 2.3.4.1). The PRINSEQ interactive program
425 (66) was used to generate additional summary statistics on each assembly.

426 A k-mer number identity was added to each contig's Trinity ID, all five assemblies were
427 concatenated, and the Evidential Gene program was used to create a single non-redundant
428 assembly. Evidential Gene relies on the Transdecoder.LongOrfs method, identifies the longest
429 ORFs, removes fragments, and uses a BLAST on self to identify highly similar sequences (98%).
430 The main (okay) and alternative (okalt) sets output from Evidential Gene were combined into a
431 final FASTA file used as the transcriptome for all subsequent analyses. Bam files, sorted bam
432 files, bam index files, and idxstats.txt files were created using samtools (67). This assembly is
433 publicly available at NCBI (Bioproject: PRJNa376023, SUB8325660). The metajinomics python
434 mapping tools (68) were used to generate a counts matrix.

435 ***Coverage Analysis***

436 Samtools was used to extract the sequencing depth at every base position for each contig
437 in every cricket sample, and a python script was used to extract the mean and standard deviation
438 of depth for each contig. The package plotly in R (69) was used to plot the depth of each cricket
439 sample. Graphs were visually compared to determine outliers. Two outliers, 1C1 and 7C2, were
440 removed.

441 EdgeR and DESeq were used to run the differential expression analysis, (35,37). The
442 raw read counts generated for each of the libraries, excluding the outliers and the backfill
443 conditions, were used as input to both programs. Similar filtering and normalization functions
444 were used in both programs to exclude any contigs that did not have at least one count per
445 million in at least two libraries. Comparisons between control and deafferented samples were
446 performed at each time point to create lists of upregulated and downregulated genes with a p
447 value cutoff of 0.05. Pairwise comparison results were then compared across time points and
448 were then compared and visualized between the two programs. Another set of lists containing the
449 genes overlapping the two programs was created for continued analysis. The EnhancedVolcano
450 package available in R was used to visualize differential gene expression in volcano plots (70).

451 ***PCR Confirmation***

452 Six sequences were randomly selected for amplification and Sanger sequencing in order
453 to validate the assembly. Sets of primers were designed to obtain the sequence of most of each
454 sequence as predicted by the Trinity assembly. Primers, available on request, were designed for
455 TRINITY21_DN57089_c8_g2_i1.p1 (hypothetical coiled-coil domain protein),
456 TRINITY21_DN58301_c9_g1_i8.p1 (eukaryotic translation initiation factor 4 gamma 3-like),
457 TRINITY25_DN131062_c0_g1_i1.p1 (protein unc-13 homolog 4B),

458 TRINITY27_DN140563_c0_g1_i5.p1 (syntaxin-binding protein 5),
459 TRINITY32_DN141398_c1_g1_i7.p1 (cytochrome P450 301a1),
460 TRINITY21_DN54942_c12_g1_i5.p1 (kinesin light chain). cDNA derived from RNA purified
461 form independent control and deafferented prothoracic ganglion samples was used for PCR. PCR
462 amplicons were gel purified and sequenced, and sequences were aligned and analyzed in
463 Geneious Prime Software (Version 2019.2.3).

464 ***BLAST Searches***

465 A Perl script was used to extract differentially expressed sequences. The NCBI BLASTx
466 local tool (71) was used to identify proteins similar to the translated nucleotide query sequences.
467 An E-value cutoff of 1e-3 was used and max target sequences was set to 1, and max hits per
468 sequence was set to 1, resulting in the output of only the top hit. Query sequences were
469 BLASTed against the entire non-redundant database downloaded from the NCBI website on
470 August 2, 2018.

471 ***Gene Ontology Analysis***

472 The program, BLAST2GO provided GO annotations for differentially regulated genes
473 (38) using the following parameters: BLASTx-fast against the nr database, number of blast
474 BLAST hits = 20, E-value of 1.0 e -3, word size of 6, hsp length cutoff of 33, with default
475 mapping and annotation settings. GO terms found to be associated with various genes were
476 manually grouped according to GO subtype (cellular component, biological process, or
477 molecular function) and plotted to view the distribution across time points. The web-based
478 CateGOrizer program was used to batch analyze each set of GO terms and determine the number
479 of GO terms under higher order GO classes of interest (72). WEGO 2.0 (Web Gene Ontology
480 Annotation Plot) with a GO level of 2 was also used to plot histograms of the GO annotations for

481 the differentially regulated genes (45). To further analyze the differentially expressed genes, an
482 enrichment analysis was performed with Metascape (61). A multiple gene list analysis looking at
483 the enrichment of the three classes of Gene Ontology terms was performed using *Drosophila*
484 *melanogaster* as the analysis species.
485
486 **Availability of data and material**
487 Initial description of assembly of this transcriptome in Fisher et al., 2018. Re-assembly was
488 completed as described above and is publicly available at NCBI (Bioproject: PRJNa376023,
489 SUB8325660)
490
491 **Availability of supporting data**
492 Supporting data are included as Supplemental Materials and on NCBI.
493
494 **Additional files:**
495 Files listing all up- and downregulated genes found to be significant at or below p=0.05 by both
496 DESeq2 and EdgeR, by just DESeq2 (DESonly), or by just EdgeR (EDRonly) are included in
497 Supplemental Materials.
498
499 **Ethics approval and consent to participate**
500 All experimental protocols were approved by Bowdoin College's IACUC committee, and all
501 experimental methods were carried out in accordance with approved guidelines and regulations.
502 Experimental design and methods reporting were carried out in compliance with ARRIVE
503 guidelines.

Consent for publication

N/A

Competing interests

The authors declare that they have no competing interests

Funding

Research reported in this project was supported by an Institutional Development Award (IDeA) from the National Institute of General Medical Sciences of the National Institutes of Health under grant number P20GM103423.

Authors' contributions

HF, assisted by LL, collected tissue and HF completed the original transcriptome assembly; FW and MM reassembled using multiple K-mers, compacted the new transcriptome using Evigene and did the differential expression analysis; JB, JJJ, LSMP, and TAM completed the sanger sequencing analysis; FW wrote the paper; JO and SK consulted on the statistical differential expression analysis; HWH obtained funding for this project and contributed to the writing. All authors read and approved the final manuscript

Acknowledgements

We thank Marko Melendy for animal care support.

References

1. Prigge CL, Kay JN. Dendrite morphogenesis from birth to adulthood. Current Opinion in Neurobiology. 2018 Dec 1;53:139–45.

2. Sampaio-Baptista C, Sanders Z-B, Johansen-Berg H. Structural Plasticity in a with motor learning and stroke rehabilitation. Annual Review of Neuroscience. 2018;41(1):25–40.

3. Brodfuehrer PD, Hoy RR. Effect of auditory deafferentation on the synaptic connectivity of a pair of identified interneurons in adult field crickets. J Neurobiol. 1988;19(1):17–38.

4. Horch HW, Sheldon E, Cutting CC, Williams CR, Riker DM, Peckler HR, et al. Bilateral consequences of chronic unilateral deafferentation in the auditory system of the cricket *Gryllus bimaculatus*. Dev Neurosci. 2011;33(1):21–37.

5. Schmitz B. Neuroplasticity and phonotaxis in monaural adult female crickets (*Gryllus bimaculatus* de Geer). Journal of Comparative Physiology A: Neuroethology. 1989;164(3):343–58.

6. Popov AV, Markovich AM, Andjan AS. Auditory interneurons in the prothoracic ganglion of the cricket, *Gryllus bimaculatus* deGeer. J Comp Physiol. 1978 Jun 1;126(2):183–92.

7. Poulet JFA, Hedwig B. Tympanic membrane oscillations and auditory receptor activity in the stridulating cricket *Gryllus bimaculatus*. Journal of Experimental Biology. 2001;204(7):1281–93.

8. Wohlers DW, Huber F. Topographical organization of the auditory pathway within the prothoracic ganglion of the cricket *Gryllus campestris* L. Cell Tissue Res. 1985;239(3):555–65.

9. Hoy RR, Nolen TG, Casaday GC. Dendritic sprouting and compensatory synaptogenesis in an identified interneuron following auditory deprivation in a cricket. Proc Natl Acad Sci USA. 1985;82(22):7772–6.

10. Schildberger K, Wohlers DW, Schmitz B. Morphological and physiological changes in central auditory neurons following unilateral foreleg amputation in larval crickets. Journal of Comparative Neurology. 1986;158:291–300.

11. Ylla G, Nakamura T, Itoh T, Kajitani R, Toyoda A, Tomonari S, et al. Cricket genomes: the genomes of future food [Internet]. Genomics; 2020 Jul [cited 2020 Aug 6]. Available from: http://biorxiv.org/lookup/doi/10.1101/2020.07.07.191841

12. Bando T, Ishimaru Y, Kida T, Hamada Y, Matsuoka Y, Nakamura T, et al. Analysis of RNA-Seq data reveals involvement of JAK/STAT signaling during leg regeneration in the cricket *Gryllus bimaculatus.* Development. 2013;140(5):959–64.

13. Zeng V, Extavour CG. ASGARD: an open-access database of annotated transcriptomes for emerging model arthropod species. Database (Oxford). 2012;2012:bas048.

14. Zeng V, Ewen-Campen B, Horch HW, Roth S, Mito T, Extavour CG. Developmental gene discovery in a hemimetabolous insect: *De novo* assembly and annotation of a transcriptome for the cricket *Gryllus bimaculatus*. Dearden PK, editor. PLoS ONE. 2013;8(5):e61479.

15. Fisher HP, Pascual MG, Jimenez SI, Michaelson DA, Joncas CT, Quenzer ED, et al. De novo assembly of a transcriptome for the cricket *Gryllus bimaculatus* prothoracic ganglion: An invertebrate model for investigating adult central nervous system compensatory plasticity. PLoS ONE. 2018;13(7):e0199070.

16. Dickson BJ. Molecular mechanisms of axon guidance. Science. 2002 Dec 6;298(5600):1959–64.

17. Tessier-Lavigne M, Goodman CS. The Molecular Biology of Axon Guidance. Science. 1996 Nov 15;274(5290):1123–33.

18. Harel NY, Strittmatter SM. Can regenerating axons recapitulate developmental guidance during recovery from spinal cord injury? Nat Rev Neurosci. 2006;7(8):603–16.

19. Kikuchi K, Kishino A, Konishi O, Kumagai K, Hosotani N, Saji I, et al. *In vitro* and *in vivo* characterization of a novel semaphorin 3A inhibitor, SM-216289 or xanthofulvin. J Biol Chem. 2003;278(44):42985–91.

20. Yu H-H, Araj HH, Ralls SA, Kolodkin AL. The transmembrane semaphorin Sema I is required in *Drosophila* for embryonic motor and CNS axon guidance. Neuron. 1998;20:207–20.

21. Gilbert D. EvidentialGene: mRNA Transcript Assembly Software [Internet]. EvidentialGene: tr2aacds, mRNA Transcript Assembly Software. 2013 [cited 2020 Jan 8]. Available from: http://arthropods.eugenes.org/EvidentialGene/trassembly.html

22. Pfister A, Johnson A, Ellers O, Horch HW. Quantification of dendritic and axonal growth after injury to the auditory system of the adult cricket *Gryllus bimaculatus*. Front Physiol. 2013;3:367.

23. Surget-Groba Y, Montoya-Burgos JI. Optimization of de novo transcriptome assembly from next-generation sequencing data. Genome Res. 2010 Oct 1;20(10):1432–40.

24. Zhao Q-Y, Wang Y, Kong Y-M, Luo D, Li X, Hao P. Optimizing de novo transcriptome assembly from short-read RNA-Seq data: a comparative study. BMC Bioinformatics. 2011;12(Suppl 14):S2.

25. Haznedaroglu BZ, Reeves D, Rismani-Yazdi H, Peccia J. Optimization of de novo transcriptome assembly from high-throughput short read sequencing data improves functional annotation for non-model organisms. BMC Bioinformatics. 2012;13(1):170.

26. Mamrot J, Legaie R, Ellery SJ, Wilson T, Seemann T, Powell DR, et al. De novo transcriptome assembly for the spiny mouse (Acomys cahirinus). Sci Rep. 2017 Dec;7(1):8996.

27. Cerveau N, Jackson DJ. Combining independent de novo assemblies optimizes the coding transcriptome for nonconventional model eukaryotic organisms. BMC Bioinformatics. 2016 Dec;17(1):525.

28. Gilbert DG. Longest protein, longest transcript or most expression, for accurate gene reconstruction of transcriptomes? [Internet]. Bioinformatics; 2019 Nov [cited 2020 Jan 9]. Available from: http://biorxiv.org/lookup/doi/10.1101/829184

29. Gan HM, Austin C, Linton S. Transcriptome-guided identification of carbohydrate active enzymes (CAZy) from the Christmas Island Red Crab, *Gecarcoidea natalis* and a vote for the inclusion of transcriptome-derived crustacean CAZys in comparative studies. Mar Biotechnol. 2018;20(5):654–65.

30. Richardson MF, Sequeira F, Selechnik D, Carneiro M, Vallinoto M, Reid JG, et al. Improving amphibian genomic resources: a multitissue reference transcriptome of an iconic invader. GigaScience [Internet]. 2018 Jan 1 [cited 2020 Jan 9];7(1). Available from: https://academic.oup.com/gigascience/article/doi/10.1093/gigascience/gix114/4662864

31. Rivera-García L, Rivera-Vicéns RE, Veglia AJ, Schizas NV. De novo transcriptome assembly of the digitate morphotype of *Briareum asbestinum* (Octocorallia: Alcyonacea) from the southwest shelf of Puerto Rico. Marine Genomics. 2019;47:100676.

32. Raplee ID, Evsikov AV, Marín de Evsikova C. Aligning the aligners: Comparison of RNA sequencing data alignment and gene expression quantification tools for clinical breast cancer research. Journal of Personalized Medicine. 2019;9(2):18.

33. Varet H, Brillet-Guéguen L, Coppée J-Y, Dillies M-A. SARTools: A DESeq2- and EdgeR-based R pipeline for comprehensive differential analysis of RNA-seq data. PLOS ONE. 2016 Jun 9;11(6):e0157022.

34. Evans C, Hardin J, Stoebel DM. Selecting between-sample RNA-Seq normalization methods from the perspective of their assumptions. Briefings in Bioinformatics. 2018 Sep 28;19(5):776–92.

35. Love MI, Huber W, Anders S. Moderated estimation of fold change and dispersion for RNA-seq data with DESeq2. Genome Biol. 2014;15(12):550.

36. Maza E, Frasse P, Senin P, Bouzayen M, Zouine M. Comparison of normalization methods for differential gene expression analysis in RNA-Seq experiments. Communicative & Integrative Biology. 2013;6(6):e25849.

37. Robinson MD, McCarthy DJ, Smyth GK. EdgeR: a Bioconductor package for differential expression analysis of digital gene expression data. Bioinformatics. 2010;26(1):139–40.

38. Gotz S, Garcia-Gomez JM, Terol J, Williams TD, Nagaraj SH, Nueda MJ, et al. High-throughput functional annotation and data mining with the Blast2GO suite. Nucleic Acids Research. 2008;36(10):3420–35.

633 39. Doughty T, Kerkhoven E. Extracting novel hypotheses and findings from RNA-seq data.
634 FEMS Yeast Res [Internet]. 2020 Mar 1 [cited 2020 Jun 11];20(2). Available from:
635 http://academic.oup.com/femsyr/article/20/2/foaa007/5721245

636 40. Zhao S, Zhang Y, Gamini R, Zhang B, von Schack D. Evaluation of two main RNA-seq
637 approaches for gene quantification in clinical RNA sequencing: polyA+ selection versus
638 rRNA depletion. Scientific Reports. 2018 Mar 19;8(1):4781.

639 41. Kucharski R, Maleszka R, Hayward DC, Ball EE. A royal jelly protein Is expressed in a
640 subset of Kenyon Cells in the mushroom bodies of the honey bee brain.
641 Naturwissenschaften. 1998;85(7):343–6.

642 42. Ferguson LC, Green J, Surridge A, Jiggins CD. Evolution of the insect yellow gene family.
643 Molecular Biology and Evolution. 2011;28(1):257–72.

644 43. Albert Š, Klaudiny J. The MRJP/YELLOW protein family of <i>Apis mellifera<i/i>
645 Identification of new members in the EST library. Journal of Insect Physiology.
646 2004;50(1):51–9.

647 44. Ye J, Fang L, Zheng H, Zhang Y, Chen J, Zhang Z, et al. WEGO: a web tool for plotting
648 GO annotations. Nucleic Acids Research. 2006;34(Web Server):W293–7.

649 45. Ye J, Zhang Y, Cui H, Liu J, Wu Y, Cheng Y, et al. WEGO 2.0: a web tool for analyzing
650 and plotting GO annotations, 2018 update. Nucleic Acids Research. 2018;46(W1):W71–5.

651 46. Quadrato G, Di Giovanni S. Waking up the sleepers: Shared transcriptional pathways in
652 axonal regeneration and neurogenesis. Cell Mol Life Sci. 2013;70(6):993–1007.

653 47. Matsunaga Y, Qadota H, Furukawa M, Choe H (Helen), Benian GM. Twitchin kinase
654 interacts with MAPKAP kinase 2 in *Caenorhabditis elegans* striated muscle. Mol Biol Cell.
655 2015;26(11):2096–111.

656 48. Baldi A, Calia E, Ciampini A, Riccio M, Vetuschi A, Persico A, et al. Deafferentation-
657 induced apoptosis of neurons in thalamic somatosensory nuclei of the newborn rat: critical
658 period and rescue from cell death by peripherally applied neurotrophins. Eur J Neurosci.
659 2000;12:2281–90.

660 49. Garcia-Valenzuela E, Gorczyca W, Darzynkiewicz Z, Sharma SC. Apoptosis in adult
661 retinal ganglion cells after axotomy. J Neurobiol. 1994 Apr;25(4):431–8.

662 50. Herman PE, Papatheodorou A, Bryant SA, Waterbury CKM, Herdy JR, Arcese AA, et al.
663 Highly conserved molecular pathways, including Wnt signaling, promote functional
664 recovery from spinal cord injury in lampreys. Sci Rep. 2018;8(1):18.

665 51. Miller CM, Page-McCaw A, Broihier HT. Matrix metalloproteinases promote motor axon
666 fasciculation in the Drosophila embryo. Development. 2008 Jan 1;135(1):95–109.

52. Kuo CT, Jan LY, Jan YN. Dendrite-specific remodeling of Drosophila sensory neurons requires matrix metalloproteases, ubiquitin-proteasome, and ecdysone signaling. Proc Natl Acad Sci USA. 2005;102(42):15230–5.

53. Zhang H, Chang M, Hansen CN, Basso DM, Noble-Haeusslein LJ. Role of matrix metalloproteinases and therapeutic benefits of their inhibition in spinal cord injury. Neurotherapeutics. 2011;8(2):206–20.

54. Horch HW, McCarthy SS, Johansen SL, Harris JM. Differential gene expression during compensatory sprouting of dendrites in the auditory system of the cricket *Gryllus bimaculatus*. Insect Molecular Biology. 2009;18(4):483–96.

55. Aoto J, Nam CI, Poon MM, Ting P, Chen L. Synaptic signaling by all-trans retinoic acid in homeostatic synaptic plasticity. Neuron. 2008;60(2):308–20.

56. Dmetrichuk JM, Carlone RL, Spencer GE. Retinoic acid induces neurite outgrowth and growth cone turning in invertebrate neurons. Dev Biol. 2006;294:39–49.

57. Maden M. Retinoic acid in the development, regeneration and maintenance of the nervous system. Nature Reviews Neuroscience. 2007;8(10):755–65.

58. Scott JG, Wen Z. Cytochromes P450 of insects: the tip of the iceberg. Pest Management Science. 2001;57(10):958–67.

59. Chavez VM, Marques G, Delbecque JP, Kobayashi K, Hollingsworth M, Burr J, et al. The Drosophila disembodied gene controls late embryonic morphogenesis and codes for a cytochrome P450 enzyme that regulates embryonic ecdysone levels. Development. 2000;127(19):4115–26.

60. Liebrich W (Universitat U, Durnberger BB, Hoffmann KH. Ecdysone 20-monooxygenase in a cricket (*Gryllus bimaculatus* ensifera, Gryllidae): activity throughout adult life cycle. Comparative biochemistry and physiology : A [Internet]. 1991 [cited 2021 Feb 5]; Available from: https://agris.fao.org/agris-search/search.do?recordID=US9150408

61. Zhou Y, Zhou B, Pache L, Chang M, Khodabakhshi AH, Tanaseichuk O, et al. Metascape provides a biologist-oriented resource for the analysis of systems-level datasets. Nature Communications. 2019;10(1):1523.

62. Anthoney N, Foldi I, Hidalgo A. Toll and Toll-like receptor signalling in development. Development [Internet]. 2018 [cited 2020 Apr 17];145(9). Available from: https://dev.biologists.org/content/145/9/dev156018

63. Li G, Forero MG, Wentzell JS, Durmus I, Wolf R, Anthoney NC, et al. A Toll-receptor map underlies structural brain plasticity. Bellen HJ, Banerjee U, editors. eLife. 2020 Feb 18;9:e52743.

64. McIlroy G, Foldi I, Aurikko J, Wentzell JS, Lim MA, Fenton JC, et al. Toll-6 and Toll-7 function as neurotrophin receptors in the *Drosophila melanogaster* CNS. Nature Neuroscience. 2013;16(9):1248–56.

65. Ballard SL, Miller DL, Ganetzky B. Retrograde neurotrophin signaling through Tollo regulates synaptic growth in Drosophila. J Cell Biol. 2014 Mar 31;204(7):1157–72.

66. Schmieder R, Edwards R. Quality control and preprocessing of metagenomic datasets. Bioinformatics. 2011 Mar 15;27(6):863–4.

67. Li H, Handsaker B, Wysoker A, Fennell T, Ruan J, Homer N, et al. The sequence alignment/map format and SAMtools. Bioinformatics. 2009;25(16):2078–9.

68. Choi J. Metajinomics mapping tool. 2017; Available from: https://github.com/metajinomics/mapping_tools

69. Sievert C. Interactive Web-Based Data Visualization with R, plotly, and shiny [Internet]. Chapman and Hall/CRC; 2020. Available from: https://plotly-r.com

70. Blighe K, Rana S, Lewis M. EnhancedVolcano: Publication-ready volcano plots with enhanced colouring and labeling. [Internet]. 2020 [cited 2020 Jan 7]. Available from: https://github.com/kevinblighe/EnhancedVolcano

71. Altschul SF, Gish W, Miller W, Myers EW, Lipman DJ. Basic local alignment search tool. Journal of Molecular Biology. 1990;215(3):403–10.

72. Hu Z, Bao J, Reecy J. CateGOrizer: A web-based program to batch analyze gene ontology classification categories. Online Journal of Bioinformatics. 2008;9:108–12.

Figure legends

Figure 1. Summary of workflow for multi k-mer assembly.

Figure 2. Volcano plot of differential gene expression in *G. bimaculatus* prothoracic ganglia at three different time points after deafferentation. The horizontal dotted line marks a p-value of 0.05, and the vertical dotted line marks no predicted fold change. Each point represents a contig determined to be differentially regulated by EdgeR or DESeq2. Blue points represent the contigs determined to be significantly regulated.

Figure 3: Correlation of fold-changes predicted by EdgeR and DESeq2 for upregulated transcripts (left) and downregulated transcripts (right) at one, three, and seven days.

Figure 4. Differentially regulated genes across three time points. Similar patterns in relative numbers of differentially regulated genes are observed between the two programs. a) EdgeR identified downregulated genes b) EdgeR identified upregulated genes c) DESeq2 identified downregulated genes d) DESeq2 identified upregulated genes.

Figure 5. Differentially regulated genes compared across the two analytical programs, DESeq2 and EdgeR. The number of genes found to be differentially regulated by both programs varies by condition.

Figure 6. Percentage of sequences with no BLAST hits, BLAST hits, and BLAST hits with additional GO term mapping. Distribution of sequences varies across times points and regulation.

Figure 7. GO term analysis organized into the three root classes: cellular component (CC), molecular function (MF), and biological process (BP). The top 5 represented GO terms across all time points in each class are represented. Many highly represented GO terms were found in the CC class whereas a broader range of GO terms were found in the MF and BP classes.

Figure 8. WEGO histograms with the distribution of Gene Ontology terms grouped by cellular component, molecular function, or biological process. a) GO terms associated with downregulated genes across all time points. b) GO terms associated with upregulated genes across all time points. Percentages are noted on the left and the number of genes within the given list that were annotated with the GO term/child term are noted on the right. On the right axis, the top numbers (olive) corresponds to the one-day data, the middle numbers, (magenta) corresponds to the three-day data, and the bottom numbers correspond to the seven-day data (teal).

764 Figure 9. Heatmap of enrichment terms as determined by Metascape. Colored by p-value as
765 indicated at the top.
766

Figures

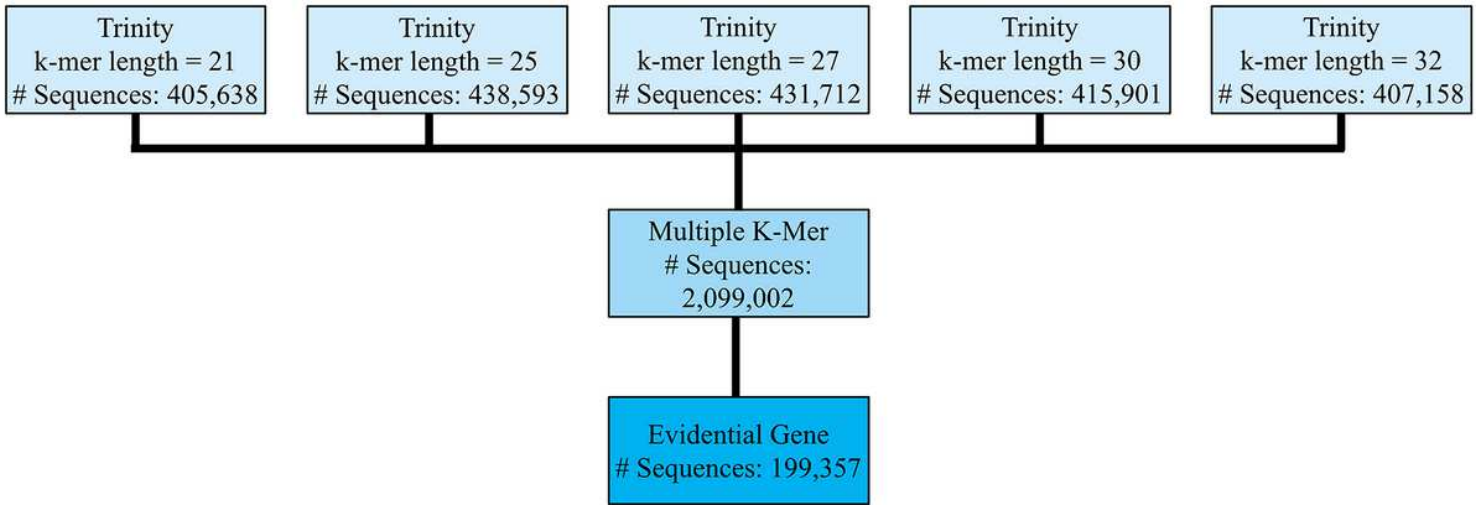

Figure 1

Summary of workflow for multi k-mer assembly.

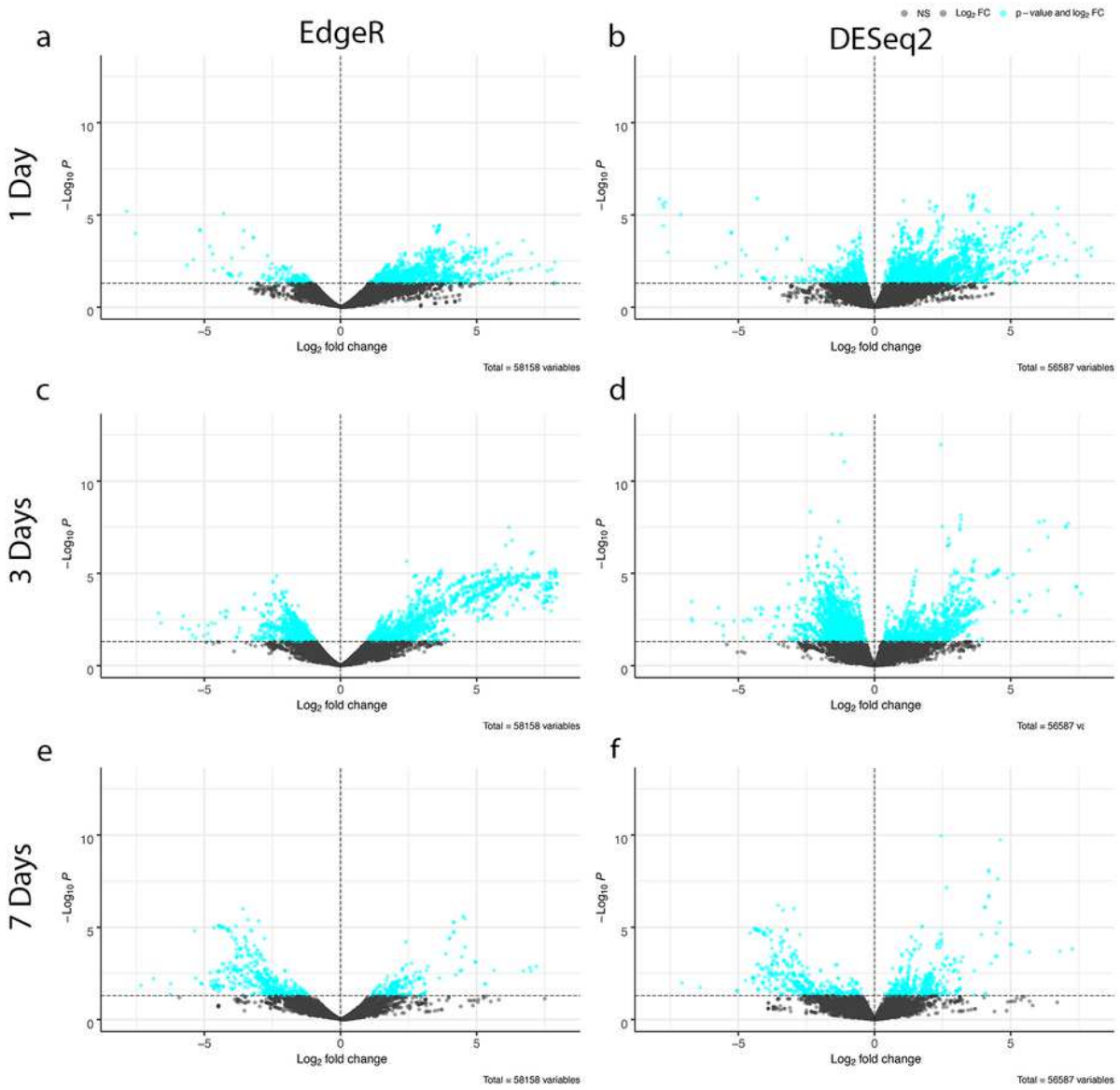

Figure 2

Volcano plot of differential gene expression in G. bimaculatus prothoracic ganglia at three different time points after deafferentation. The horizontal dotted line marks a p-value of 0.05, and the vertical dotted line marks no predicted fold change. Each point represents a contig determined to be differentially regulated by EdgeR or DESeq2. Blue points represent the contigs determined to be significantly regulated.

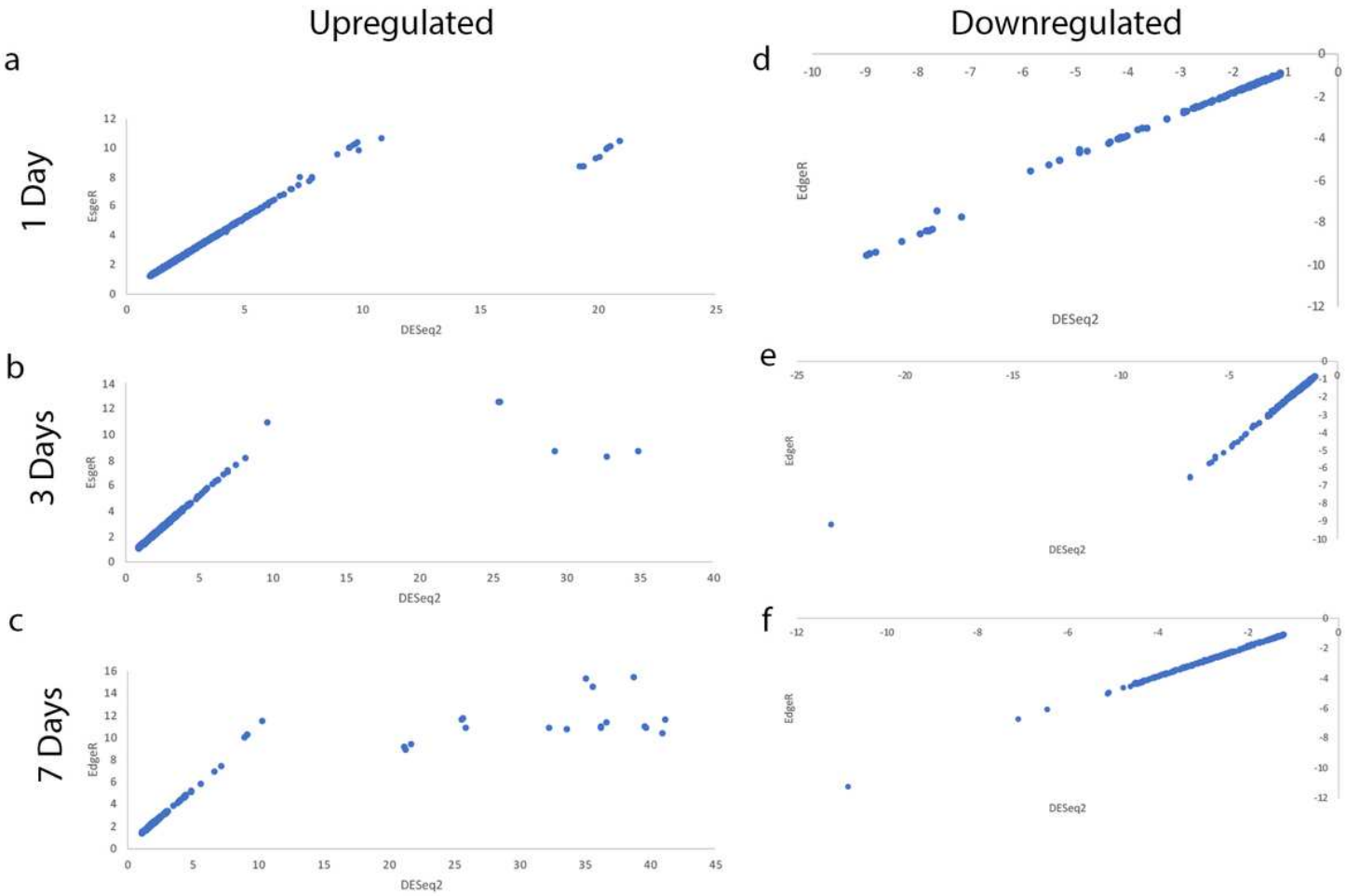

Figure 3

Correlation of fold-changes predicted by EdgeR and DESeq2 for upregulated transcripts (left) and downregulated transcripts (right) at one, three, and seven days.

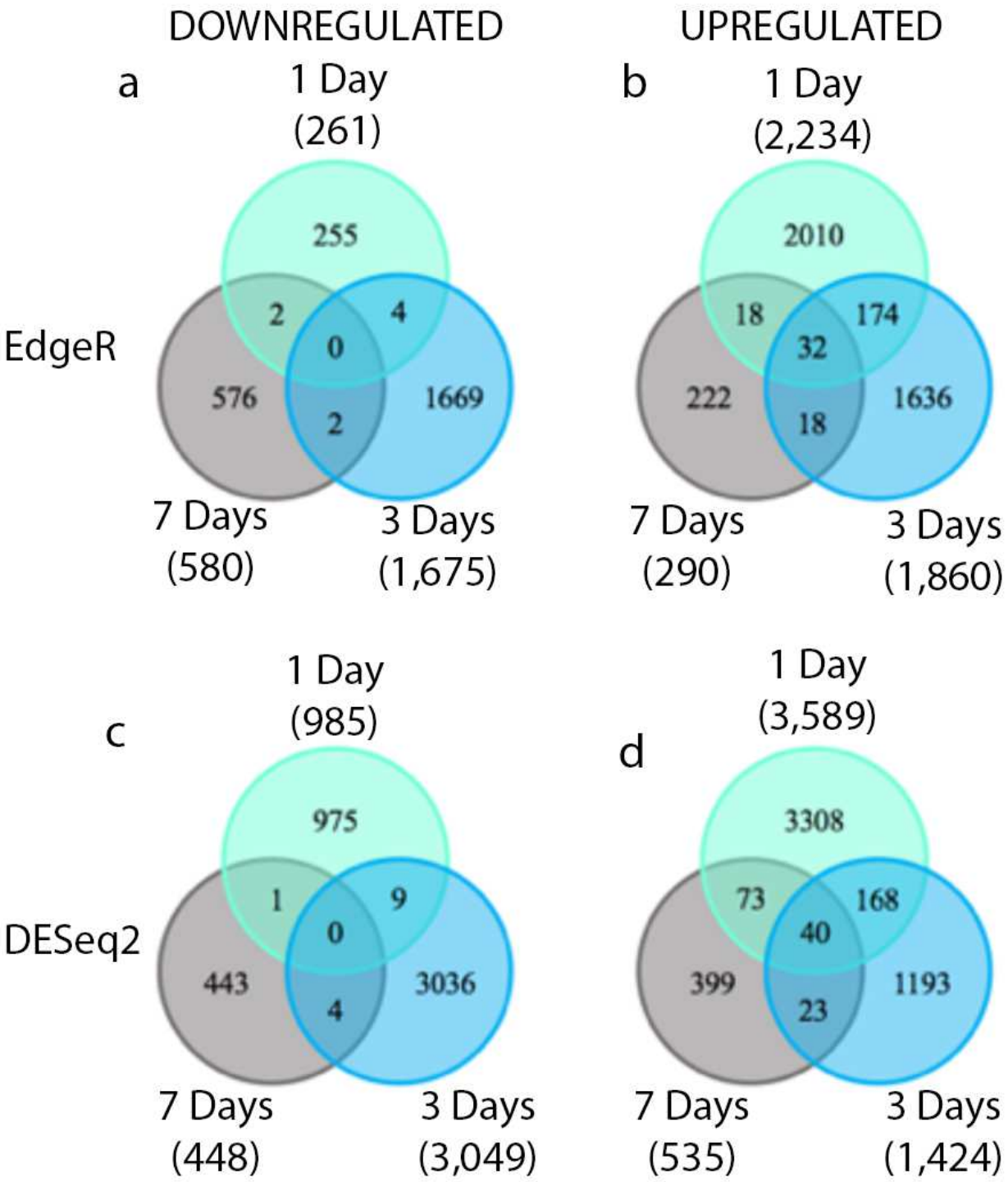

Figure 4

Differentially regulated genes across three time points. Similar patterns in relative numbers of differentially regulated genes are observed between the two programs. a) EdgeR identified downregulated genes b) EdgeR identified upregulated genes c) DESeq2 identified downregulated genes d) DESeq2 identified upregulated genes.

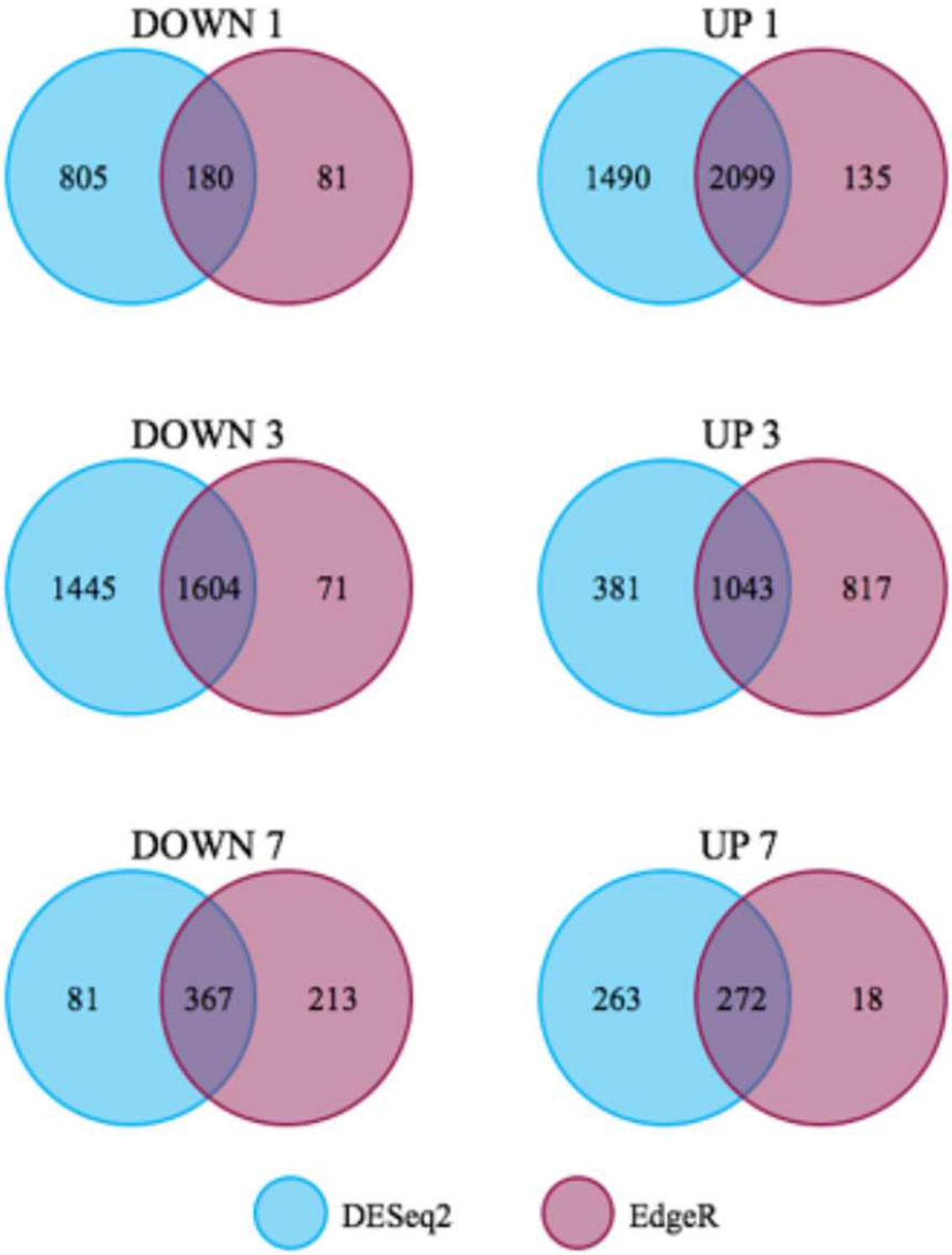

Figure 5

Differentially regulated genes compared across the two analytical programs, DESeq2 and EdgeR. The number of genes found to be differentially regulated by both programs varies by condition.

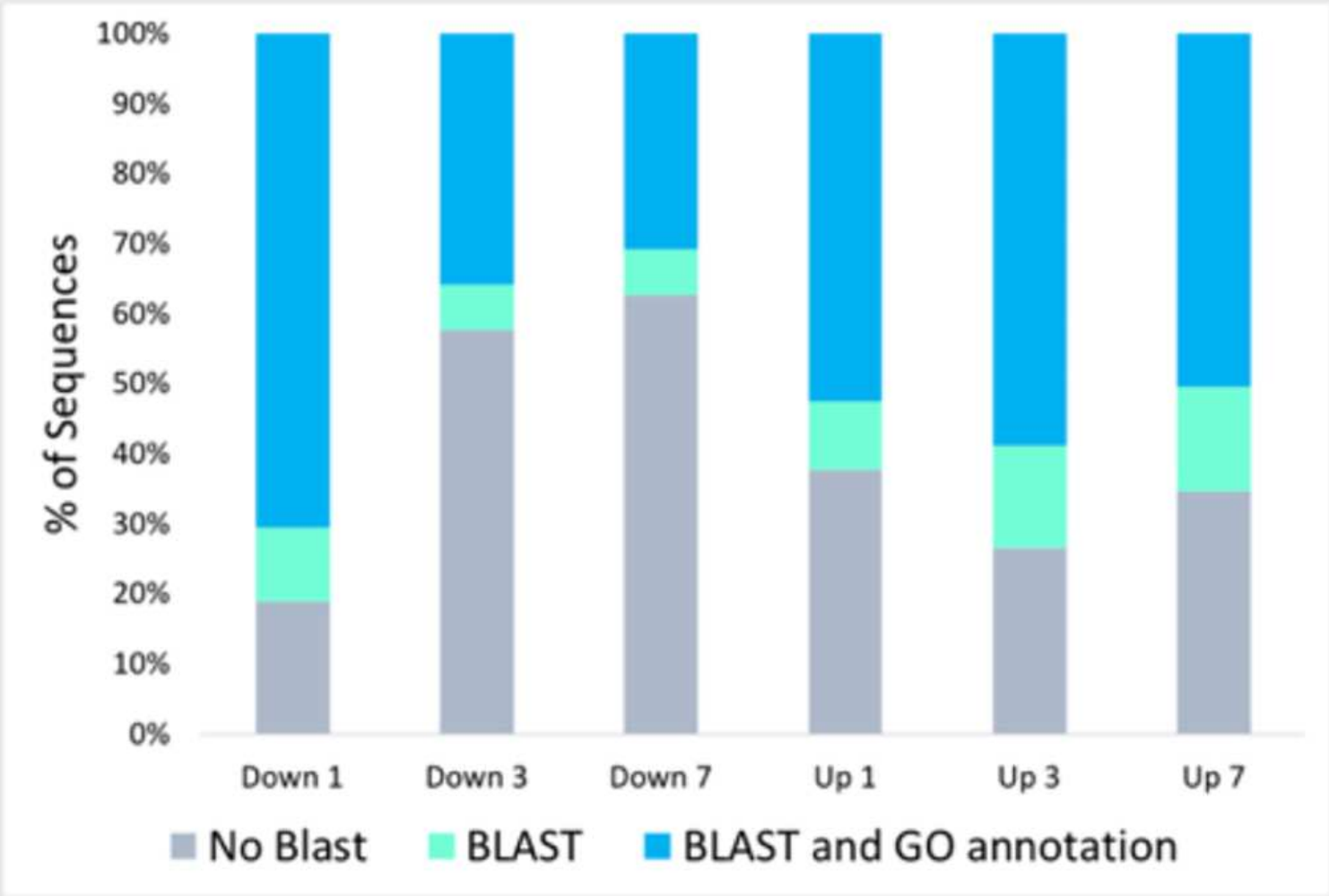

Figure 6

Percentage of sequences with no BLAST hits, BLAST hits, and BLAST hits with additional GO term mapping. Distribution of sequences varies across times points and regulation.

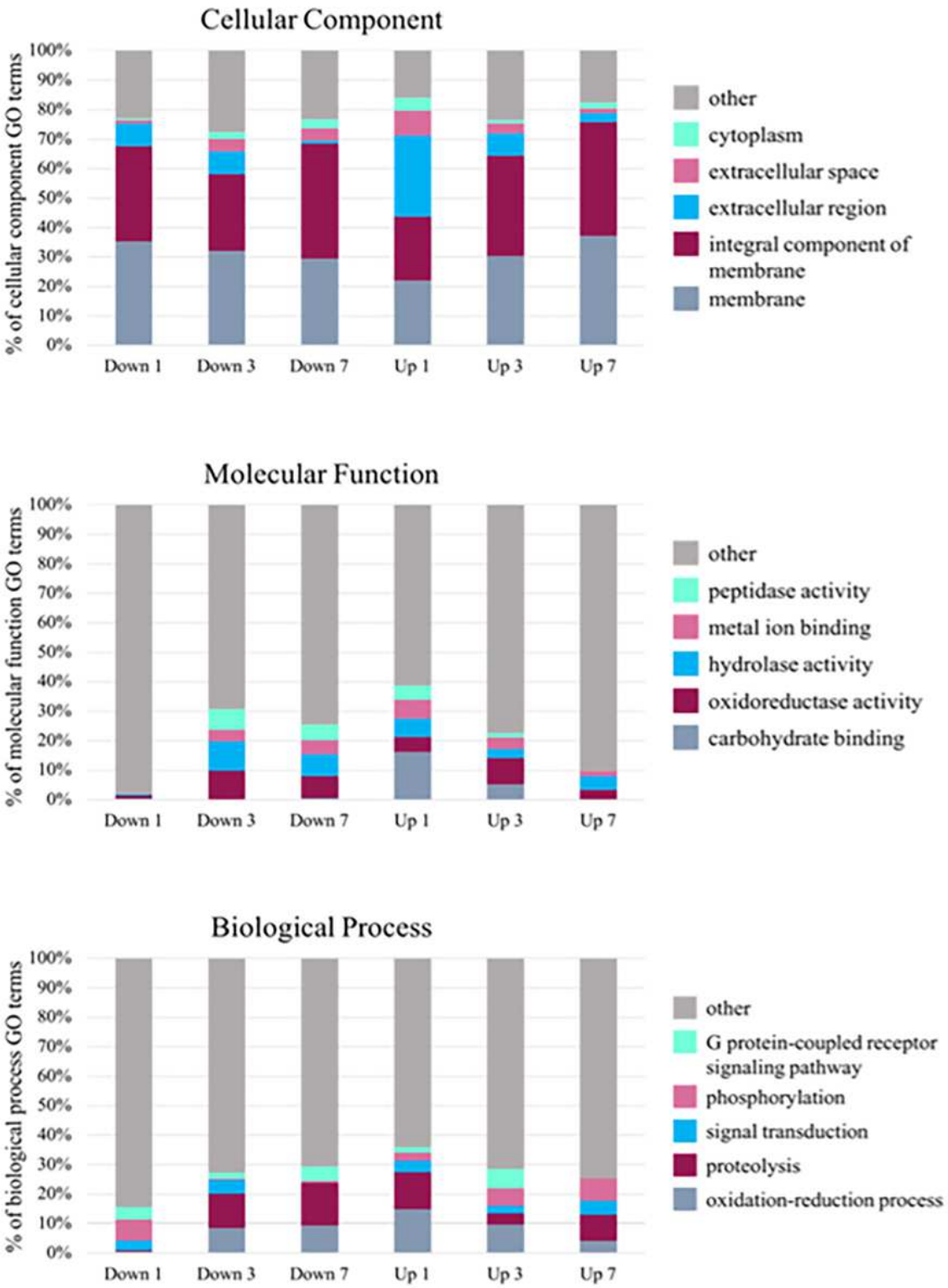

Figure 7

GO term analysis organized into the three root classes: cellular component (CC), molecular function (MF), and biological process (BP). The top 5 represented GO terms across all time points in each class are represented. Many highly represented GO terms were found in the CC class whereas a broader range of GO terms were found in the MF and BP classes.

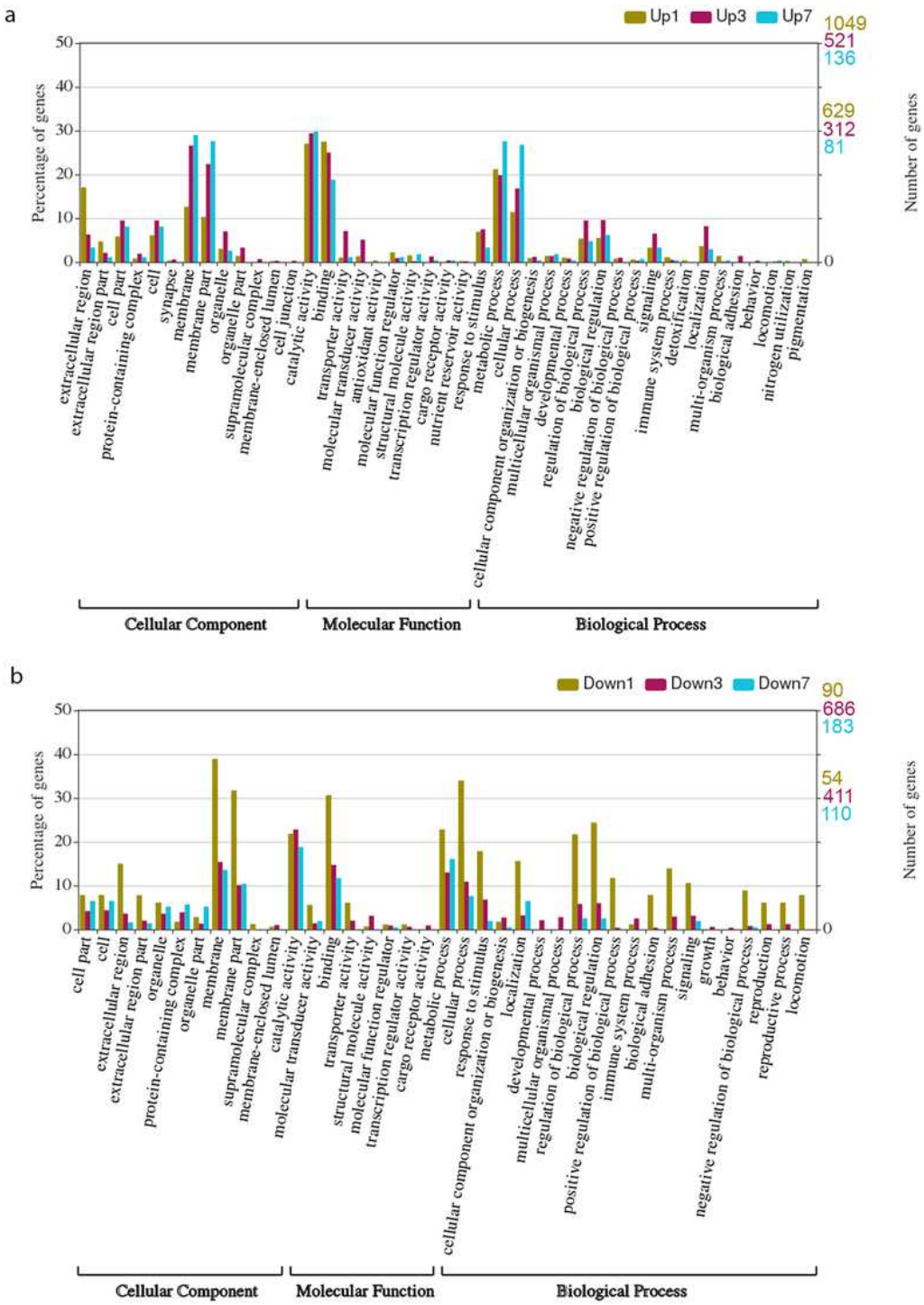

Figure 8

WEGO histograms with the distribution of Gene Ontology terms grouped by cellular component, molecular function, or biological process. a) GO terms associated with downregulated genes across all time points. b) GO terms associated with upregulated genes across all time points. Percentages are noted on the left and the number of genes within the given list that were annotated with the GO term/child term are noted on the right. On the right axis, the top numbers (olive) corresponds to the one-day data, the

middle numbers, (magenta) corresponds to the three-day data, and the bottom numbers correspond to the seven-day data (teal).

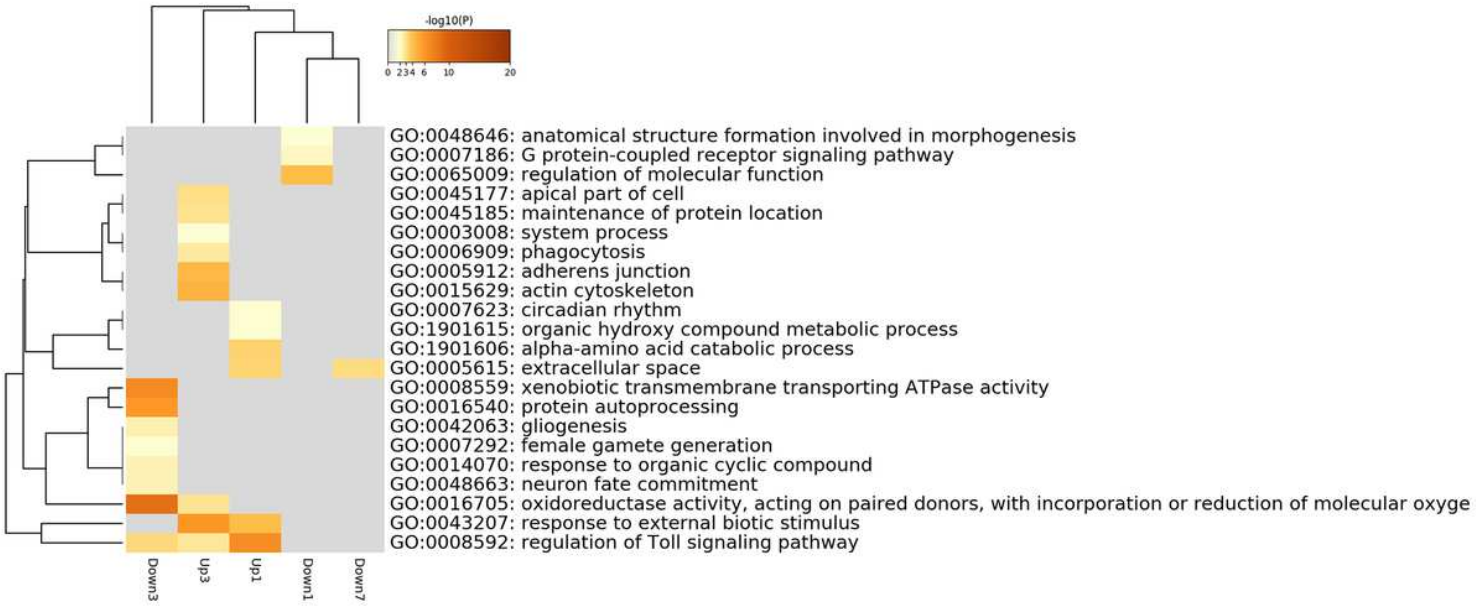

Figure 9

Heatmap of enrichment terms as determined by M etascape. Colored by p-value as indicated at the top.

Supplementary Files

This is a list of supplementary files associated with this preprint. Click to download.

- SupplementalMaterialsTitlePage.pdf